

Brain

A missense mutation in the murine Opa3 gene models human Costeff syndrome

Vanessa J. Davies, Kate A. Powell, Kathryn E. White, Wanfen Yip, Vanessa Hogan, Andrew J. Hollins, Jennifer R. Davies, Malgorzata Piechota, David G. Brownstein, Stuart J. Moat, Philip P. Nichols, Michael A. Wride, Michael E. Boulton and Marcela Votruba

Brain 131:368-380, 2008.

doi:10.1093/brain/awm333

The full text of this article, along with updated information and services is available online at <http://brain.oxfordjournals.org/cgi/content/full/131/2/368>

References

This article cites 33 references, 12 of which can be accessed free at <http://brain.oxfordjournals.org/cgi/content/full/131/2/368#BIBL>

Cited by

This article has been cited by 1 articles at 15 May 2008 . View these citations at <http://brain.oxfordjournals.org/cgi/content/full/131/2/368#otherarticles>

Reprints

Reprints of this article can be ordered at <http://brain.oxfordjournals.org/cgi/reprintform>

Email and RSS alerting

Sign up for email alerts, and subscribe to this journal's RSS feeds at <http://brain.oxfordjournals.org>

PowerPoint® image downloads

Images from this journal can be downloaded with one click as a PowerPoint slide.

Journal information

Additional information about Brain, including how to subscribe can be found at <http://brain.oxfordjournals.org>

Published on behalf of

Guarantors of Brain
<http://www.oup.co.uk/>

A missense mutation in the murine *Opa3* gene models human Costeff syndrome

Vanessa J. Davies,¹ Kate A. Powell,¹ Kathryn E. White,² Wanfen Yip,¹ Vanessa Hogan,² Andrew J. Hollins,¹ Jennifer R. Davies,¹ Malgorzata Piechota,¹ David G. Brownstein,³ Stuart J. Moat,⁴ Philip P. Nichols,² Michael A. Wride,^{1,5} Michael E. Boulton^{1,6} and Marcela Votruba⁷

¹School of Optometry and Vision Sciences, Cardiff University, Cardiff, ²Neurology, Medical School, Newcastle upon Tyne, ³Research Animal Pathology Core Facility, University of Edinburgh, UK, ⁴Department of Medical Biochemistry and Immunology, University Hospital of Wales, Cardiff, UK, ⁵Zoology Department, School of Natural Sciences, University of Dublin Trinity College, Dublin 2, Ireland, ⁶Department of Ophthalmology and Vision Sciences, University of Texas Medical Branch, Galveston, TX, USA and ⁷Cardiff Eye Unit, University Hospital Wales, Cardiff, UK

Correspondence to: Marcela Votruba, School of Optometry and Vision Sciences, Cardiff University, Maindy Road, Cathays, Cardiff CF24 4LU, UK

E-mail: votrubam@cardiff.ac.uk

Opa3 mRNA is expressed in all tissues examined to date, but currently the function of the OPA3 protein is unknown. Intriguingly, various mutations in the OPA3 gene lead to two similar diseases in humans: autosomal dominant inherited optic atrophy and cataract (ADOAC) and a metabolic condition; type 3-methylglutaconic aciduria (MGA). Early onset bilateral optic atrophy is a common characteristic of both disorders; retinal ganglion cells are lost and visual acuity is impaired from an early age. In order to investigate the function of the OPA3 protein, we have generated a novel ENU-induced mutant mouse carrying a missense mutation in the OPA3 gene. The heterozygous mutation in exon 2, causes an amino acid change p.L122P (c.365T>C), which is predicted to alter tertiary protein structure. In the heterozygous state, the mice appear uncompromised however; in the homozygous state mice display some of the features of MGA. Visual function is severely reduced, consistent with significant loss of retinal ganglion cells and degeneration of axons in the optic nerve. In the homozygous optic nerve, there was evidence of increased mitochondrial activity, as demonstrated by the increased presence of mitochondrial marker Cytochrome C Oxidase (COX) histochemistry. Mice homozygous for the opa3^{L122P} mutation also display a severe multi-systemic disease characterized by reduced lifespan (majority dying before 4 months), decreased weight, dilated cardiomyopathy, extrapyramidal dysfunction and gross neuro-muscular defects. All of these defects are synonymous with the phenotypic characteristics of Type III MGA found in humans. This model will be of major importance for future studies of the specific function of the OPA3 gene.

Keywords: OPA3; inherited optic atrophy; 3-methylglutaconic aciduria; mouse model

Abbreviations: ADOA = autosomal dominant optic atrophy; ADOAC = autosomal dominant optic atrophy and cataract; CMT4A = Charcot–Marie–Tooth type 4A; CMT2A = Charcot–Marie–Tooth type 2A; COX = cytochrome C oxidase; DAB = 3,3'-diaminobenzidine; ENU = N-ethyl-N-nitrosourea; FRDA = Friedreich's ataxia; H&E = haematoxylin and eosin; HMSN VI = hereditary motor and sensory neuropathy type VI; INL = inner nuclear layer; IPL = inner plexiform layer; mfn = mitofusin; MGA = type 3-methylglutaric aciduria; MRC = medical research council; MTP = mitochondrial trifunctional protein; NBF = neutral buffered formalin; NF = neurofilament; NFL = nerve fibre layer; MRI = magnetic resonance imaging; OKN = optokinetic drum; ONL = outer nuclear layer; PINK1 = PTEN-induced kinase I; RGCs = retinal ganglion cells; SmithKline Beecham Pharmaceuticals; Harwell, MRC Mouse Genome Centre and Mammalian Genetics Unit; Imperial College School of Medicine at St Mary's; Royal London Hospital, St Bartholomew's and the Royal London School of Medicine; Phenotype Assessment (SHIRPA)

Received September 21, 2007. Revised December 17, 2007. Accepted December 18, 2007

Introduction

Hereditary optic atrophy encompasses a group of disorders with varying modes of inheritance in which optic atrophy is a primary characteristic. Autosomal dominant optic atrophy [ADOA; OMIM 165500; (Votruba *et al.*, 1998a, b)] is the most common of these disorders, and is characterized by progressive loss of visual acuity, central scotoma, colour vision defects, bilateral loss of retinal ganglion cells (RGCs) and ascending atrophy of the optic disc (Kjer, 1959). To date, over 100 mutations in the *OPA1* gene, which localizes to chromosome 3q28-q29, have been identified as responsible for ADOA (<http://ibbma.univ-angers.fr/eOPA1>). More rarely, ADOA has been linked to mutations in the *OPA3* gene. In this instance, a blue-dot cerulean cataract accompanies dominantly inherited optic neuropathy [ADOAC; OMIM 165300; (Garcin *et al.*, 1961; Reynier *et al.*, 2004)]. Two dominant missense mutations have been identified in the *OPA3* gene: one causes a heterozygous 277G>A transition in exon 2 (c.277G>A) change and the other a heterozygous 313C>G transversion in exon 2 (c.313C>G) (Reynier *et al.*, 2004).

Mutations in the *OPA3* gene are also responsible for another syndrome with bilateral optic atrophy as a primary characteristic, that of type III 3-methylglutaconic aciduria [MGA; OMIM 25801; (Anikster *et al.*, 2001)]. Two homozygous mutations are reported: G→C change at the -1 position of intron 1 in the 3' (acceptor) splice site (c.143-1G>C) (Anikster *et al.*, 2001) and the in frame deletion c.320_337del (AGCAGCGCCACAAGGAGG) (Kleta *et al.*, 2002). Type III MGA (Costeff syndrome) is one of four disorders that comprise MGA, a rare neuro-ophthalmological syndrome characterized by increased urinary excretion of 3-methylglutaconic acid and 3-methylglutaric acid, early-onset bilateral optic atrophy, pallor of the optic disc, reduced visual acuity, late onset spasticity, extra pyramidal dysfunction and cognitive deficit. Type I MGA is a mild neurological disease that results from a deficiency in 3-methylglutaconyl-CoA hydratase in the leucine-oxidation pathway. Type II MGA (Barth syndrome) is an X-linked disorder that consists of dilated cardiomyopathy, short stature and neutropenia. Finally, Type IV MGA is a moderate to severe neurological disease that is associated with cardiac, ophthalmic, hepatic and renal symptoms.

The unique existence of type III MGA in a subset of Iraqi-Jews and its distinct phenotype led to the mapping of the gene responsible for this disorder, *OPA3*, to chromosome 19q13.2–q13.3 (Nystuen *et al.*, 1997), and the identification of the founder mutation (Anikster *et al.*, 2001). The *OPA3* gene contains two exons and encodes for a mitochondrial-related protein of unknown function (Da Cruz *et al.*, 2003). mRNA is ubiquitously expressed throughout the body and in many regions of the brain (Anikster *et al.*, 2001).

The distinct, yet common characteristics shared by MGA type III and ADOAC, and the variable mode of

inheritance of these disorders has shed little light on the possible function of the *OPA3* protein. Proteomics suggest that *OPA3* localizes to the inner membrane of the mitochondria (Da Cruz *et al.*, 2003), while fibroblasts from a patient with ADOAC are particularly susceptible to apoptosis (Reynier *et al.*, 2004). However, little more than this is known about *Opa3* protein function, since no abnormalities in the respiratory chain, mitochondrial membrane potential or morphology of the mitochondrial network were identified in these fibroblasts [in contrast to what is known of the consequences of *OPA1* haploinsufficiency; (Olichon *et al.*, 2003; Cipolat *et al.*, 2004; Griparic *et al.*, 2004)].

In order to understand the function of the *OPA3* protein and its role in disease, we generated a novel mouse model by ENU mutagenesis, carrying a point mutation in the *OPA3* gene. Our model contains a missense mutation that is predicted to alter the tertiary structure of the *OPA3* protein by creating an amino acid change from leucine to proline at position 122. In the heterozygous state, these mice are indistinguishable from wild-type littermate controls. However, homozygous mutant animals display a severe multi-systemic disease, characterized by retinal abnormality and optic atrophy, reduced lifespan, decreased weight, dilated cardiomyopathy, extra-pyramidal dysfunction and gross neuro-muscular defects. The loss of vision displayed by these mice was consistent with degeneration of axons in the optic nerve. Thus, we have generated a mutant *Opa3* murine model that displays a clinical phenotype comparable to Type III MGA.

Material and Methods

Genotype analysis

Opa3 genotyping was performed using specific primers from *mOpa3* exon2 (Forward 5'-GCACGAAGATGCGCATAATGG-3' and reverse 5'-GTACAGTGAGCATTGCAGACC-3'; product size 343 bp).

Cycling conditions were 35 cycles of 1 min denature at 92°C, 1 min anneal at 63°C and 1 min extension at 72°C with a final extension at 72°C for 5 min.

The 343-bp product was digested using Pst1 enzyme (sequence CTGCAG; 10 U/μl) giving a 205-bp product from the wild-type (T) allele and a 247-bp product from the recessive (C) allele (Fig. 1).

Rd1 genotyping was carried out as a multiplex reaction, with the following three primers in equal combination: RD3: 5'-TGACAATTACTCCTTTCCCTCAGTCTGA-3', RD4: 5'-GTAAACA GCAAGAGGCTTTATTGGGAAC-3', and RD6: 5'-TACCCACCCCTTCCTAATTTTCTCAGC-3' (Gimenez and Montoliu, 2001; Qiao *et al.*, 2003). The wild-type *Rd1* allele was 300 bp and the mutant allele was 450 bp (Davies *et al.*, 2007).

Breeding strategy and embryo analysis

pa3 and *rd1* allele-specific PCR genotyping was used to direct breeding with wild-type C57Bl/6JCrI mice and the removal of the *rd1* allele of *pdeB* (carried by the C3H paternal line) was thus ensured. *Opa3*^{+/−} 'founder' mice were crossed with C57Bl/6JCrI

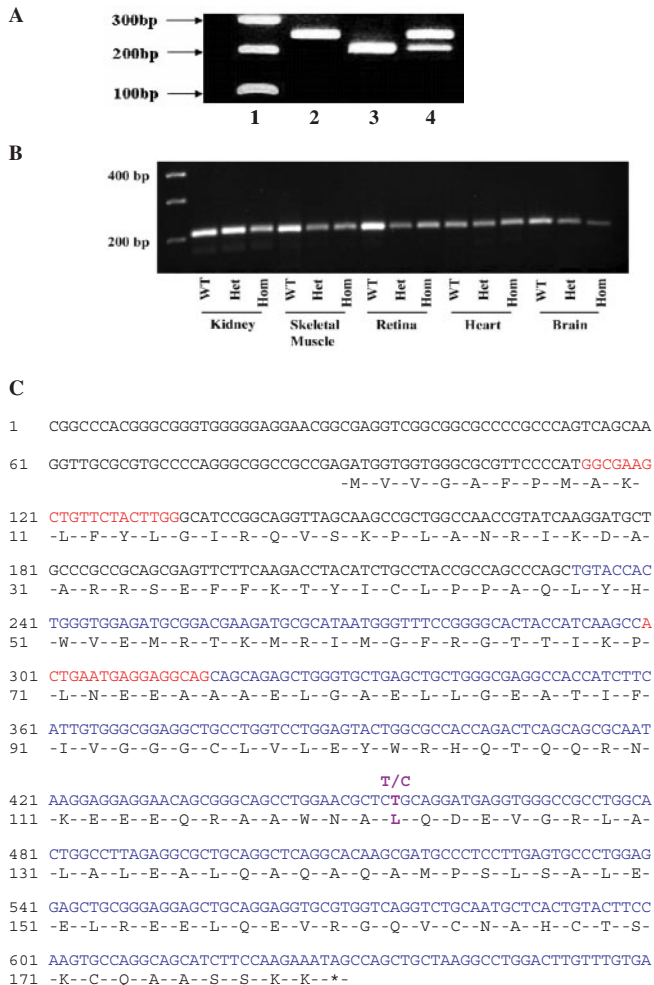


Fig. 1 (A) Two per cent Agarose gel showing: (i) Hyperladder IV DNA ladder (Bioline, UK), (ii) *Opa3*^{-/-} band 247 bp, (iii) *Opa3*^{+/+} band 205 bp, (iv) *Opa3*^{+/-} bands 247 bp and 205 bp. (B) RT-PCR from kidney, skeletal muscle, retina, heart and brain of animals that were wild-type (WT, *Opa3*^{+/+}), heterozygous (Het, *Opa3*^{+/-}) and homozygous (Hom, *Opa3*^{-/-}) for the mutation. *Opa3* mRNA is therefore produced ubiquitously in all tissues tested and is unaffected by the presence of the T>C mutation. (C) Mouse *Opa3* cDNA and amino acid sequences (Ensembl gene product ENSMUSG0000052214; RefSeq peptide: NP.997408.2.; RefSeq DNA: NM.207525.2) indicating the position of primers used for RT-PCR, and showing the position of the T>C change introduced by ENU mutagenesis which results in a leucine to proline shift at position 122 of the peptide. Exon 1, black; exon 2 blue; forward and reverse primers red. Peptide marked below cDNA. T/C mutation, purple (amino acid L>P at position 122).

mice (Charles River, UK) to move the mutation to a C57Bl/6JCrI background. This was continued at G1 to G4. *Opa3*^{+/-} F1 and F2 mice were inter-crossed to obtain homozygous *Opa3*^{-/-} mice for further immediate analysis.

RT-PCR

Total RNA was isolated from mouse retina, kidney, brain, skeletal muscle and heart of *Opa3*^{+/+}, *Opa3*^{+/-} and *Opa3*^{-/-} littermates using the RNeasy Mini kit (Qiagen, UK). First-strand cDNA

synthesis was performed using a cDNA synthesis kit (BioLine) with Oligo (dT)₁₈ primers. PCR was performed using 20 pmol mOpa3 primers designed to span an intron/exon boundary (forward 5'-GGCGAAGCTGTTCTACTTGG; reverse 5'-CTGCTGCCTCTCATTCACT) and a *Taq* polymerase mastermix (BioMix Red; BioLine, UK). Cycling conditions as above, giving a final product of 202-bp.

Functional visual testing

Animals

Opa3^{-/-} ($n=7-9$), *Opa3*^{+/-} ($n=12-16$) and *Opa3*^{+/+} ($n=10-15$) mice were tested at 3–4 months age on the SHIRPA primary neurological screen and the optokinetic drum (OKN) task. Founder *Opa3*^{+/-} ($n=6$) and littermate controls ($n=6$) were also tested at 8 and 12 months of age.

SHIRPA primary screen and clinical examination of the eye

Mice were assessed on 36 separate screening tests that form part of the SHIRPA primary protocol (Rogers *et al.*, 1997). This included tests of muscle tone, power and coordination, and hearing, using a click box (90 dB and 18–20 Hz). Behaviours were ranked according to a standard behavioural score (http://www.mgu.har.mrc.ac.uk/facilities/mutagenesis/mutabase/shirpa_1.html).

Statistical analysis to assess any differences between groups was performed using parametric *t*-test or non-parametric Mann-Whitney U-test, where appropriate.

Slit lamp biomicroscopy (Haag Streit) was performed on restrained, but non-sedated mice with pupillary dilation (1% atropine MINIMS) in order to examine the anterior segment and lens. Indirect ophthalmoscopy, employing a Volk Super field and 66 D lens, was used to visualize the fundus.

OKN

Mice were tested on the optokinetic response test with the use of a rotating OKN. A digital video camera (JVC, GR-D250) linked to a monitor and DVD recorder was used to record movements (<http://www.eumorphia.org/>) (Thaung *et al.*, 2002; Hart *et al.*, 2005). Briefly, mice were placed on the platform and allowed to settle for 2 mins. The drum was rotated for 1 min and the mice were observed for a head-tracking response. After a 30-s break, the drum was rotated in the opposite direction for 1 min. The mice were presented with a 2° grating corresponding to 0.25 cycles/degree. If an animal failed to track the grating it was tested again on two separate occasions; if the animal still failed to track the grating it was tested on the 4° and 8° grating (0.125 and 0.0625 cycles/degree, respectively). The performance of the founder *Opa3*^{+/-} animals was statistically analysed using *t*-test. To validate the protocol and technique in our hands we first tested sighted C57Bl/6JCrI mice ($n=3$) and non-sighted C3H ($n=3$) mice on the OKN.

Biochemical Investigations

Urine samples were obtained from 12-month-old *Opa3*^{+/-} founders ($n=6$) and littermate controls ($n=6$). Blood samples extracted from 3–4-month-old *Opa3*^{-/-} ($n=3$), *Opa3*^{+/-} ($n=3$), *Opa3*^{+/+} ($n=3$) mice.

Histology

Eyes were enucleated from 3-month-old *Opa3*^{+/-} (*n* = 3), *Opa3*^{-/-} (*n* = 3) and *Opa3*^{+/+} (*n* = 3) littermate control mice. The eyes were fixed at 4°C in 10% neutral buffered formaldehyde (NBF), dehydrated through a graded ethanol series and embedded in paraffin wax (RA Lamb, UK) for serial sectioning at 7 µm. Coronal sections were taken at 1 in 20 intervals and haematoxylin & eosin (H&E) stained in order to identify the optic nerve. Five retinal sections either side of the optic nerve were then mounted and alternately stained with H&E. Images were taken of each section using a Leica DMR microscope and a Leica DC500 camera with Qwin software for manual RGC counts. Individual retinal layer thickness was measured using the Qwin software.

Brain, heart, skeletal muscle, liver, kidney and spleen from 4–5-month-old *Opa3*^{-/-} (*n* = 4), *Opa3*^{+/-} (*n* = 4) and *Opa3*^{+/+} (*n* = 5) littermate controls were fixed in 10% NBF for wax histology and stained with picros red to demonstrate collagen, or with H&E or Cresyl violet.

Magnetic resonance imaging (MRI)

To examine the fat distribution within the 3-month-old mice, ‘healthy’ *Opa3*^{+/+} (*n* = 1), *Opa3*^{+/-} (*n* = 1) and *Opa3*^{-/-} (*n* = 1) mice with a ‘sick’ *Opa3*^{-/-} mouse (*n* = 1) were imaged using a Bruker Biospin Advance 9.4T (400 MHz) MRI system (Etlingen, Germany). The mice were culled and positioned inside a 35-mm quadrature whole-body mouse coil. For each animal a series of RARE scans with a RARE factor of 1 (55 slices, 0.5-mm thickness) were run in coronal orientation. The weighting of the images was designed to be of proton-density: repetition time: 500 ms; echo time: 12.6 ms, and were imaged with a field of view 7.0 × 3.5 cm² and a matrix size 512 × 256. The images were acquired with and without fat suppression, at the same receiver gain, and reconstructed with the same scaling. The fat distribution images were then created by subtracting the fat suppressed image from the unsuppressed image.

Electron microscopy

Optic nerves, brain and spinal cord from 3-month-old *Opa3*^{-/-} (*n* = 3) *Opa3*^{+/-} (*n* = 3) and *Opa3*^{+/+} (*n* = 3) mice were fixed in a mixture of 4% paraformaldehyde and 5% glutaraldehyde in cacodylate buffer, post-fixed in 1% osmium tetroxide, dehydrated in acetone and embedded in epoxy resin. Ultrathin sections from optic nerve, spinal cord and brain corpus callosum were stained with uranyl acetate and lead citrate and examined using a Philips CM100 transmission electron microscope (EM Research Services, Newcastle University). Images (×19 000) were taken of 15 random areas per optic nerve from three *Opa3*^{+/+} and three *Opa3*^{-/-} mice. The appearance of the mitochondrial matrix was described as either ‘clear’ or ‘opaque’ depending on intensity of staining (Fig. 7G and H). The number density (*N_v*) of mitochondria in the optic nerve was estimated from the high magnification images (Andrews *et al.*, 2006).

Neurofilament and cytochrome C oxidase (COX) histochemistry

For neurofilament (NF) staining, tissues were fixed in 4% PFA in 0.1 M phosphate buffer pH 7.4 for 15 min at 4°C. Endogenous biotin was blocked on sections using a commercially available kit (Vector laboratories, UK). A mouse monoclonal primary antibody

to NF-H (Novocastra, UK) was used in conjunction with an animal research kit (DAKO ARK™ kit) to minimize reactivity of anti-mouse secondary antibody with endogenous immunoglobulin. Sections were first incubated with peroxidase block from the DAKO ARK™ kit for 5 min, followed by biotinylated primary NF-H antibody in a humidified chamber for 30 min, then with streptavidin-peroxidase reagent from the kit for 30 min in a humidified chamber. Reaction product was visualized using 3,3'-diaminobenzidine (DAB) from the DAKO ARK™ kit for 5 min, washed, dehydrated, cleared in HistoClear™ and mounted in DPX™. Images were taken on a digital camera using ImagePro Plus.

For COX histochemistry 10 µm longitudinal serial sections were cut from optic nerve and brain samples taken from 3-month-old *Opa3*^{-/-} (*n* = 3) *Opa3*^{+/-} (*n* = 3) and *Opa3*^{+/+} mice (*n* = 3). Sections were processed for COX histochemistry to assess cellular enzyme activity (Old and Johnson, 1989) by incubating in a medium containing 4 mM DAB, 100 µM cytochrome c in 0.1 M phosphate and catalase for 35 min at 37°C. Images were obtained using a Zeiss Axioplan microscope with an Axiocam HRc digital camera and axiovision image-capture software. Densitometric measurements were made using Zeiss KS-300 densitometry software in the whole optic nerve from each section stained for COX histochemistry. The densitometry scale is an inverse linear scale ranging from 0 (black) to 255 (white). Higher COX activity is reflected by an increasingly dense, insoluble indamine polymer.

Results

Generation of *Opa3* mutant mice: the p.L122P mutation

An ENU mutagenized DNA archive from 10 000 C3H male mice was screened for point mutations in *Opa3* exons 1 and 2, using heteroduplex analysis by temperature gradient capillary electrophoresis, run at two temperatures: 55–60°C and 60–70°C (Ingenium, SA). Positive fragments were sequenced and three SNPs were found, one of which was a heterozygous missense mutation in exon 2 coding for T to C transition at position 365 in the open reading frame (c.365T>C) (Fig. 1C). This mutation is predicted to cause an amino acid change within the peptide (Leucine 122 to Proline: L122P) in exon 2, which is expected to alter the tertiary protein structure. Sperm were used (IVF with C57Bl/6J females) to generate heterozygous hybrid *Opa3*^{+/-} ‘founders’ (the B6; C3-*Opa3*^{L122P} mouse line). All procedures complied with local ethical, national and international regulatory bodies.

Effects of *Opa3*^{+/-} mutation on transcription

Opa3 mRNA was present in all tissues examined and its transcription was unaffected by the presence of the T/C mutation (Fig. 1B).

Progeny

Opa3^{+/-} mutant animals are robust and indistinguishable from littermate control *Opa3*^{+/+} mice, surviving well into adulthood. They are produced with the expected ratio from

Table 1 Outcomes from outcross and inter-cross matings

	<i>Opa3</i> ^{+/-} × <i>Opa3</i> ^{+/-}	<i>Opa3</i> ^{+/+} × <i>Opa3</i> ^{+/-}
Mean litter size	8.26	8.0
Survival at weaning from birth (%)	84	93
<i>Opa3</i> ^{+/+} progeny, n (%)	25 (25)	46 (50)
<i>Opa3</i> ^{+/-} progeny, n (%)	60 (50)	54 (50)
<i>Opa3</i> ^{-/-} progeny, n (%)	15 (25)	—

Obtained and predicted (bold, in parentheses) percentages of genotypes from outcross ($n = 40$) and inter-cross ($n = 256$) mouse matings.

intercross (60%) and outcross (54%) matings (Table 1). In this generation (G1), pregnancies of carrier *Opa3*^{+/-} dams from outcross or inter-cross matings are phenotypically normal and without any complications. However, the majority of *Opa3*^{-/-} progeny are compromised from birth. Seventeen per cent die before weaning (3 weeks), with a possible gestational loss; 15% are born against an expected birth rate of 25% (Table 1). Those that survive post-weaning display a very variable phenotype. The majority die within 12–16 weeks, although two animals have survived to 7 months of age. The phenotype of these mice varies, but characteristics include: a ‘runted’ appearance at birth, stunted growth, frail appearance, cranial facial abnormalities (a snubbed snout), splayed gait and reduced activity (Fig. 2). Those *Opa3*^{-/-} mice that appear ‘normal’ at birth have a shorter life span than littermate *Opa3*^{+/-} and *Opa3*^{+/+} mice. Once *Opa3*^{-/-} mice become compromised they display piloerection, pronounced tremor, hunched physique, reduced body fat and have limited movement due to abnormal gait (Fig. 2). Animals that initially appear to be healthy deteriorate rapidly and often die within 7 days. The cause of death is not obvious, occurring suddenly in the absence of any preceding illness, undue stress or fasting. In the majority of instances, we were unable to investigate the progeny of *Opa3*^{-/-} inter-cross or outcross matings due to the frail state of the *Opa3*^{-/-} females. Two *Opa3*^{-/-} inter-crosses were set up, but pregnancy was never established, despite an extensive period allowed for mating.

Neurological defects and functional visual anomalies

A basic neurological examination of the *Opa3*^{+/+}, *Opa3*^{+/-} and *Opa3*^{-/-} mice was performed at 3–4 months of age to assess the extent of the behavioural phenotype before testing the mice for visual function. Founder *Opa3*^{+/-} and littermate *Opa3*^{+/+} mice were tested at 8 months of age, to assess whether ageing compromises the *Opa3*^{+/-} mice further. Due to deteriorating health and declining numbers, we were unable to test the *Opa3*^{-/-} mice beyond 4 months of age.

Slit lamp biomicroscopy of the lens and anterior segment and dilated fundal examination by indirect microscopy in

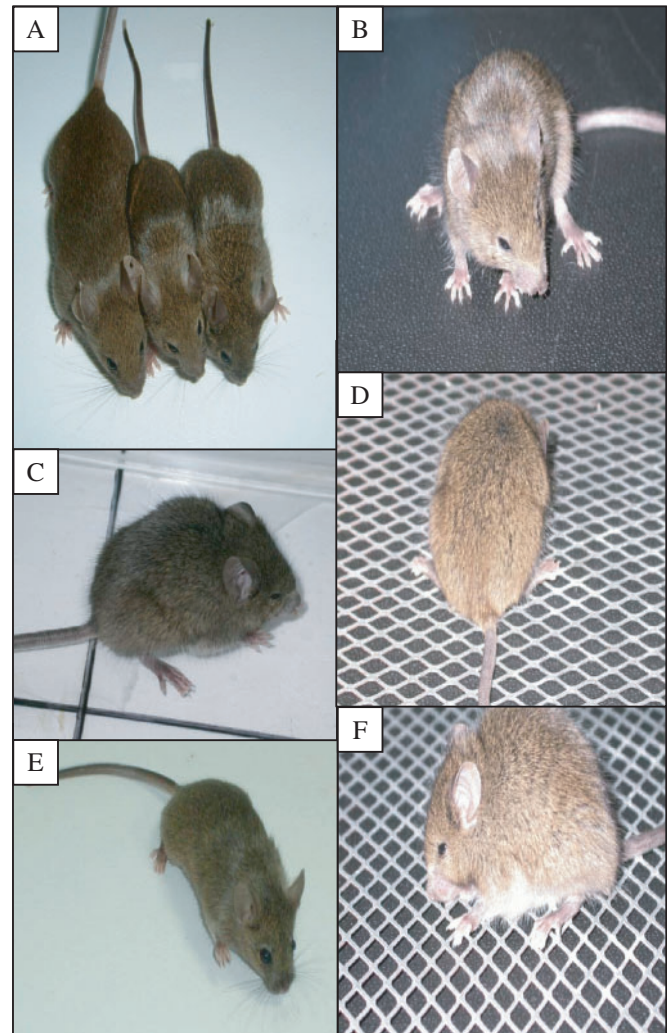


Fig. 2 Photographs demonstrating various phenotypic characteristics of the *Opa3*^{-/-} mice. (A) Shows the size difference between the *Opa3*^{+/+} mouse (left) and the two *Opa3*^{-/-} mice next to it. (B–D) and (F) shows the key phenotypic characteristics of *Opa3*^{-/-} mice: note the frail, hunched appearance, splayed gait and piloerection. (E) demonstrates the snubbed snout common in *Opa3*^{-/-} mice.

restrained, non-sedated mice was performed on all animals in the study. No evidence of cataract was seen by 8–12 months. No gross retinal anomalies were detected, within the limits of resolution possible with these techniques. The optic nerve appeared to be normal; however, its shape and size were not quantified and are particularly difficult to evaluate in mice, due to their small size.

Primary SHIRPA screen

The primary SHIRPA screen allows observational assessment of 36 different general health and neurological measures (Rogers *et al.*, 1997; <http://www.eumorphia.org>). In the 3–4-month-old *Opa3*^{+/-} mice, there was no significant effect of genotype on 35 of the separate behavioural measures. However, there was a significant

Table 2 Primary SHIRPA screen of wild-type and homozygous mutant mice

Behaviour	Opa3 ^{+/+}		Opa3 ^{-/-}	
Body position	4	Rearing on hind legs	3	Sitting or standing
Spontaneous activity	2	Vigorous scratch/groom, moderate movement	1	Casual scratch/groom, slow movement
Tremor	0	None	1	Mild
Transfer arousal	4	Momentary freeze, then swift movement	1	Prolonged freeze, then slight movement
Piloerection	0	None	0	None
Startle response	1	Preyer reflex	2	Jump <1 cm
Gait	0	Normal	1	Fluid but abnormal
Tail elevation	1	Horizontally extended	0	Dragging
Visual placing	3	Before vibrassee contact	2	Upon vibrassee contact
Toe pinch	3	Brisk, rapid withdrawal	0	None
Provoked biting	1	Present	0	Absent
Aggression	1	Provoked biting or attack	0	None

Deficits recorded in SHIRPA primary observation assessment for 3- to 4-month-old *Opa3*^{+/+} controls ($n = 10$), and *Opa3*^{-/-} mutants ($n = 9$). The median ranked behavioural score is given, together with its description in the SHIRPA primary screen.

effect of genotype on transfer arousal from the viewing jar to the open field arena $U(12,10) = 31.00$, $P < 0.05$. The *Opa3*^{-/-} mice moved more actively in the open field arena (median 4.5, interquartile range 4, 5) compared with *Opa3*^{+/+} mice (median 3.5, interquartile range 3–4).

In the 3–4-month-old *Opa3*^{-/-} mice, there was a significant effect of genotype on 14 of the 36 behavioural measures compared with *Opa3*^{+/+} littermates (Table 2, Fig. 3). *Opa3*^{-/-} mice weighed less ($t = -4.336$, $P < 0.001$; Fig. 3A) and were less active ($t = -3.636$, $P < 0.005$; Fig. 3B) than *Opa3*^{+/+} mice. In the viewing jar, *Opa3*^{-/-} mice were significantly different to *Opa3*^{+/+} mice with respect to their body position: $U(9, 10) = 13$, $P < 0.005$, spontaneous activity: $U(9, 10) = 14.00$, $P < 0.01$ and tremor: $U(9, 10) = 10.00$, $P < 0.05$ (Table 2 for description). In the arena, the *Opa3*^{-/-} mice were significantly different from *Opa3*^{+/+} mice with respect to five measures: transfer arousal from the viewing jar to the arena: $U(9, 10) = 8.5$, $P < 0.005$; startle response tested by the MRC standard click box: $U(9, 10) = 18.00$, $P < 0.05$; gait: $U(9, 10) = 5.0$, $P < 0.001$; tail elevation: $U(9, 10) = 25.0$, $P < 0.05$ and piloerection: $U(9, 10) = 25$, $P < 0.05$. For behaviours measured outside of the arena, there were significant differences between the *Opa3*^{-/-} and *Opa3*^{+/+} mice with respect to four measures: visual placing: $U(9, 10) = 18.00$, $P < 0.05$; toe response: $U(9, 10) = 17.5$, $P < 0.05$; provoked biting: $U(9, 10) = 22.5$, $P < 0.03$ and aggression: $U(9, 10) = 23.0$, $P < 0.05$. Results from this basic neurological screen suggest that *Opa3*^{-/-} mice might have compromised aspects of muscle and lower motoneuron function, spinocerebellar function, sensory function, autonomic function and neuropsychiatric function (Rogers *et al.*, 1997). Further testing is required to define the specific nature of these deficits. Importantly, locomotion and visual function appear to be compromised in the *Opa3*^{-/-} mice.

It was impossible to examine the *Opa3*^{-/-} mice beyond 4 months of age using the primary SHIRPA screen. However *Opa3*^{+/+} founder mice were tested at 8 months of age and were found to be significantly different to the *Opa3*^{+/+}

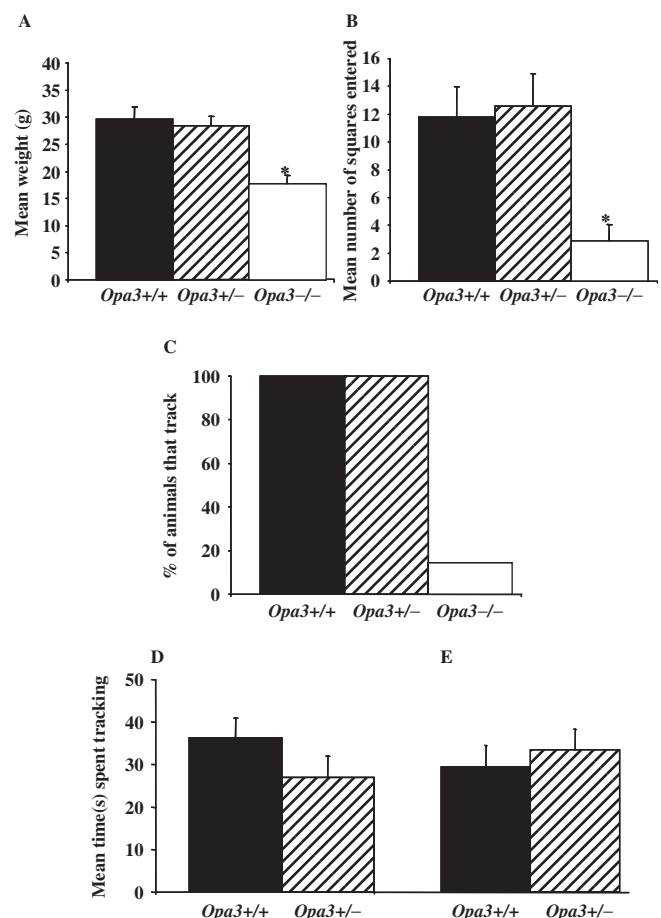


Fig. 3 Performance on the SHIRPA primary screen. Graphs showing 3–4-month *Opa3*^{+/+} ($n = 10$) control performance against the *Opa3*^{+/-} ($n = 12$) and *Opa3*^{-/-} ($n = 9$) mutants: (A) mean weight (g) \pm SEM and (B) mean locomotor activity \pm SEM. The *Opa3*^{-/-} mice had significantly lower weights and were less active compared to *Opa3*^{+/+} littermate controls, * $P < 0.05$. (C) Percentage of 3- to 4-month-old animals that track the 2° grating on the OKN, *Opa3*^{+/+} ($n = 15$), *Opa3*^{+/-} ($n = 16$), *Opa3*^{-/-} ($n = 7$). (D) and (E) Mean time (s) that founder *Opa3*^{+/+} ($n = 6$) and littermate control *Opa3*^{+/+} animals ($n = 6$) spent tracking the 2° grating, at (D) 8 months of age and (E) 12 months of age, \pm SEM

littermates only with respect to the pinna reflex: $U(6, 6) = 3.0$, $P < 0.005$. Therefore, at 8 months of age, the $Opa3^{+/-}$ mice remain relatively indistinguishable from littermate controls.

OKN test

One of the key clinical characteristics of ADOAC and Type III MGA is reduced visual acuity. For this reason, and given the impaired visual placing phenotype identified in the $Opa3^{-/-}$ mice on the primary SHIRPA screen, we examined the visual acuity of 3–4-month-old $Opa3^{-/-}$ mice. The $Opa3^{+/-}$ founder mice were tested at 8 and 12 months of age to assess any age-related deterioration in visual function of carrier mice. Sighted C57Bl/6JCrI mice were capable of tracking the moving acuity square wave grating at all frequencies (defined as at least one head tracking movement in the same direction and speed of the drum (Thaung et al., 2002)). Non-sighted C3H mice failed to track any of the gratings, confirming the validity and sensitivity of our test data [data not shown; (Hart et al., 2005)].

$Opa3^{+/-}$ and $Opa3^{+/+}$ mice at 3–4 months of age displayed normal visual function by tracking the 2° grating, consistent with the published literature [Fig. 3; (Thaung et al., 2002)]. However, only 1 out of 7 (14%) of the $Opa3^{-/-}$ mice tested tracked the 2° grating (Fig. 3C). If a mouse failed to track any grating, it was tested on the same grating on a separate occasion (<http://www.eumorphia.org/>). Non-responding $Opa3^{-/-}$ mice were tested on the 4° grating; two out of the remaining six (33%) mice tracked this grating, indicating reduced visual acuity. Finally, one of the four (25%) remaining non-responding $Opa3^{-/-}$ mice tracked the larger 8° grating. Therefore, three of the seven $Opa3^{-/-}$ mice failed to track the 2°, 4° and 8° grating, indicating that the $Opa3^{-/-}$ mice have no or limited visual function.

Older $Opa3^{+/-}$ founder mice were tested at 8 and 12 months of age using the 2° grating (Fig. 3D and E). No difference was recorded in terms of the ability to track, or time spent tracking the grating over a 2-min period between the $Opa3^{+/-}$ and $Opa3^{+/+}$ mice at either 8 months ($t = 1.378$, $P > 0.05$) or 12 months of age ($t = 10.570$, $P > 0.05$). Therefore, the $Opa3^{+/-}$ mice are not functionally blind.

Biochemistry

Increased urinary excretion of 3-methylglutaconic acid and 3-methylglutaric acid is diagnostic of type III MGA. We were unable to obtain urine from $Opa3^{-/-}$ mice owing to their poor health. $Opa3^{-/-}$ mice became extremely dehydrated despite being observed to drink normally, and we were unable to devise any strategy that would enable us to collect urine. As an alternative, blood was collected for analysis of acylcarnitines by tandem mass spectrometry, to determine if organic acids could be detected; but using this method we were unable to detect any differences between the three phenotypes. However, we were able to

test the urine of 12-month-old founder $Opa3^{+/-}$, but no differences were observed between these and littermate $Opa3^{+/+}$ mice.

General histology

In $Opa3^{-/-}$ mice, the liver was lipid/glycogen depleted. A marked cardiomyopathy was also observed and the left and right ventricular chambers were dilated (Fig. 4H). Both the interventricular septum and left ventricular free wall were thinned (Fig. 4H). The left and right ventricular myocardium had diffuse changes consisting of matrix expansion, inducing interstitial fibrosis, cardiac muscle fibre deposits, atrophy and hyperatrophy of residual muscle fibres, as well as vacuolation of muscle fibres (Fig. 4K). Such severity of cardiomyopathy would explain the observed dramatic deterioration of health and is a likely cause of death.

No gross structural abnormalities were observed between the $Opa3^{+/+}$, $Opa3^{+/-}$ or $Opa3^{-/-}$ mutant mice in the skeletal muscle, spleen or brain. Kidneys also appeared to be normal by H&E histology despite the dehydrated state of $Opa3^{-/-}$ mice; however, this analysis will only detect gross deficits.

MRI

Compromised $Opa3^{-/-}$ mice were shorter and contained less fat in the body cavity than other mice (Fig. 5). Changes in length and body fat were observed between compromised $Opa3^{-/-}$, $Opa3^{+/-}$ and $Opa3^{+/+}$ mice; however no further differences were identified. In a healthy state, the $Opa3^{-/-}$ mice appear indistinguishable from their $Opa3^{+/+}$ and $Opa3^{+/-}$ littermates (Fig. 5).

Retinal histology

A marked reduction in retinal ganglion cells (RGCs) was apparent in the RGC layer of $Opa3^{-/-}$ retina (Fig. 6A and D). At 3–4 months of age RGC counts from H&E stained retinal sections were statistically different between $Opa3^{-/-}$ and $Opa3^{+/+}$ mice ($t = -4.806$, $P < 0.01$; Fig. 6A). Furthermore, there was a considerable difference between the thicknesses of the $Opa3^{-/-}$ compared to $Opa3^{+/+}$ retinal layer (Fig. 6E–H). The whole retina, measured from retinal pigment epithelium to nerve fibre layer (NFL), was significantly thinner, with most marked differences in the inner plexiform layer (IPL), outer nuclear layer (ONL), combined RGC and NFL (Fig. 6E–H).

Retinal morphology appeared normal in the 3- to 4-month-old $Opa3^{+/-}$ mice (Fig. 6C) when compared to $Opa3^{+/+}$ littermates.

Electron microscopy and neurofilament immunostaining

Degenerating axons were observed in spinal cord, brain and, most abundantly, in optic nerve of $Opa3^{-/-}$

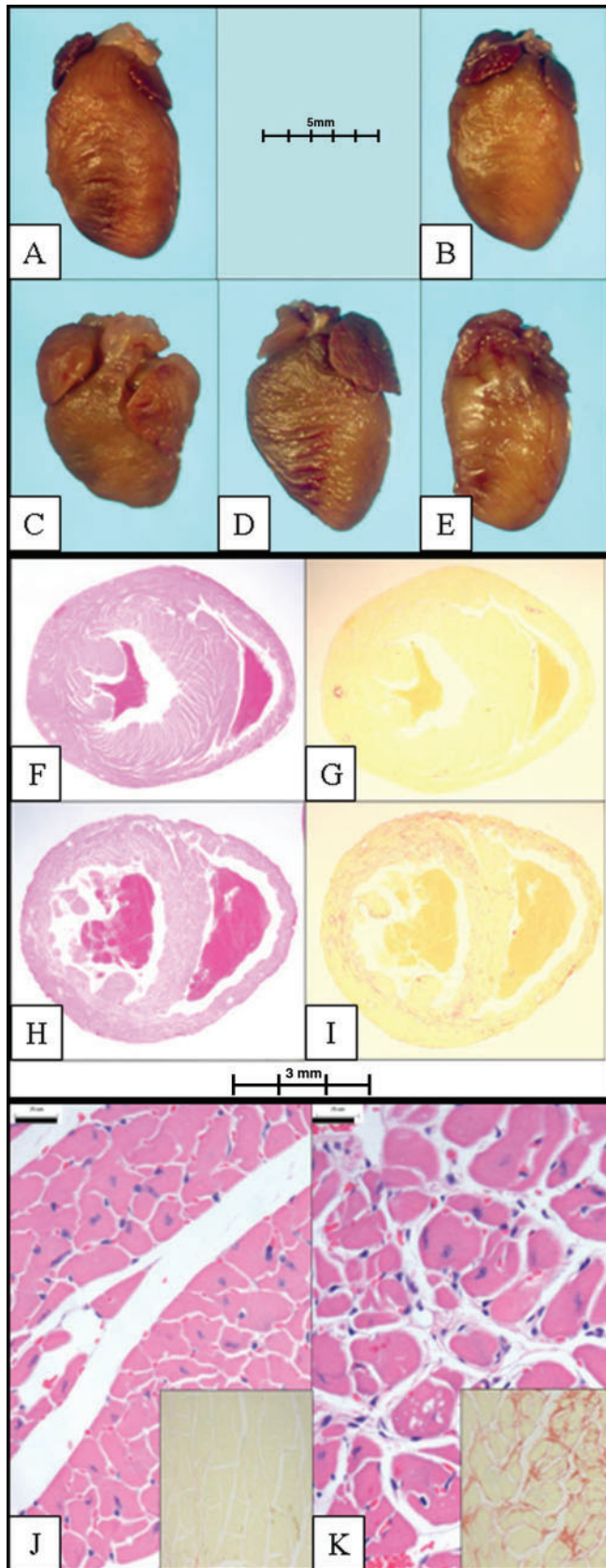


Fig. 4 Histopathology of 3- to 4-month homozygote *Opa3*^{-/-} compared with *Opa3*^{+/+} controls. (A) and (B) show the anterior

mice (Fig. 7). This type of degenerating axon is referred to as 'dark' degeneration and may be a consequence of neurofilament aggregation. To address this, neurofilament staining, using NF-H, a standard neurofilament marker, was performed on homozygous optic nerve and an increase in staining was observed (Fig. 8).

Mitochondria with either clear or opaquely stained matrix were found in both wild-type and homozygous optic nerves (Fig. 7G and H). The proportion of opaque mitochondria in the *Opa3*^{-/-} mice was significantly higher

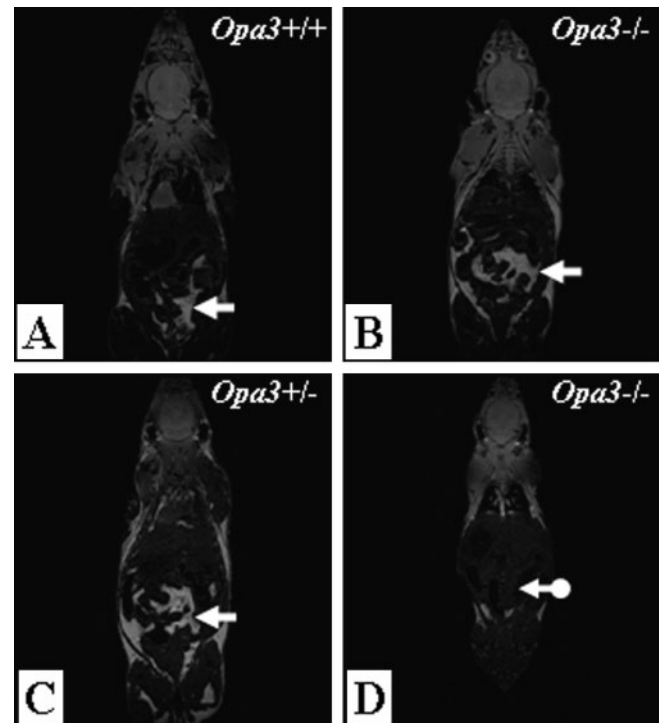


Fig. 5 Magnetic resonance images displaying the variation in abdominal body fat distribution in (A) *Opa3*^{+/+}, (B) 'healthy' *Opa3*^{-/-}, (C) *Opa3*^{+/-} and (D) 'sick' *Opa3*^{-/-} mice. The 'sick' *Opa3*^{-/-} mouse has considerably less fat compared to 'healthy' *Opa3*^{-/-}, *Opa3*^{+/-} or *Opa3*^{+/+} animals. Arrows show the position of abdominal fat in panels (A–C). Arrow in (D) shows the absence of an abdominal fat pad in compromised *Opa3*^{-/-} animals.

surface of *Opa3*^{+/+} hearts, (C–E) of *Opa3*^{-/-} hearts. Sections from *Opa3*^{-/-} hearts display reduced ventricular mass and atrial enlargement. Panels (F–I) are transverse sections through the base of the ventricles. (F) and (H) show H&E stained sections from *Opa3*^{+/+} (F) and *Opa3*^{-/-} (H) mice. Panels (G) and (I) show sections stained with picro-sirius red for collagen from *Opa3*^{+/+} (G) and *Opa3*^{-/-} (I) mice respectively. The ventricular cavities of *Opa3*^{-/-} mice are dilated and there is an increase in picro-sirius red staining in the myocardium of both chambers. Panels (J and K) are H&E stained sections showing septal myocardium from (J) *Opa3*^{+/+} and (K) *Opa3*^{-/-} animals. Panel (K) also demonstrates matrix expansion, cardiac muscle fibre dropout and vacuolation and hypertrophy of residual cardiac muscle fibres. Insets in (J) and (K) are of sections stained using picro-sirius red to demonstrate collagen in the expanded matrix.

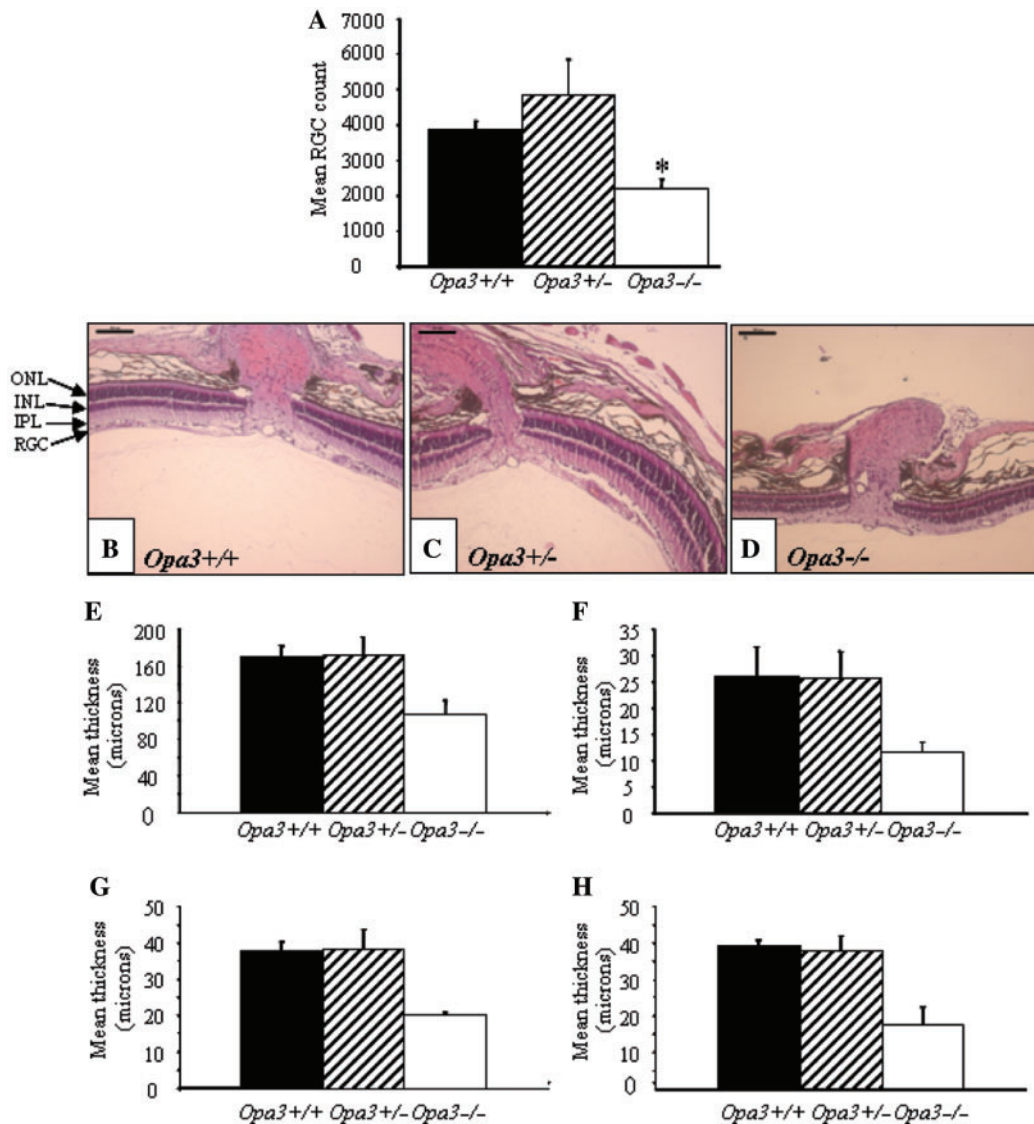


Fig. 6 Analysis of the RGC layer of *Opa3*^{-/-} mutants compared to the *Opa3*^{+/-} mutants and *Opa3*^{+/+} controls. Retinal sections were stained with haematoxylin and eosin (H&E). **(A)** Graph showing the mean \pm SEM RGC count from ten sections taken either side of the optic nerve from 3–4-month-old *Opa3*^{+/+} ($n=3$), *Opa3*^{+/-} ($n=3$) and *Opa3*^{-/-} ($n=3$). The *Opa3*^{-/-} mice have significantly fewer RGCs compared to littermate *Opa3*^{+/+} controls, $*P < 0.05$. **(B–D)** are representative H&E retinal sections from *Opa3*^{+/+}, *Opa3*^{+/-} and *Opa3*^{-/-} mice respectively. The retinal thickness is reduced in the *Opa3*^{-/-} mouse compared to littermate *Opa3*^{+/+} controls, $*P < 0.05$. Graphs displaying the mean thickness (μm) \pm SEM of the **(E)** whole retina, **(F)** combined RGC and NFL layer, **(G)** IPL and **(H)** ONL for the *Opa3*^{+/+}, *Opa3*^{+/-} and *Opa3*^{-/-} mice. Bar = 100 μm .

than in *Opa3*^{+/+} mice (mean \pm SD: 44 ± 4 versus 24 ± 8 , $P = 0.021$); however, there was no significant difference in mitochondrial number density (0.99 ± 0.4 versus $0.97 \pm 0.3 \mu\text{m}^{-3}$).

No significant abnormalities were observed by electron microscopy in the optic nerve, brain and spinal cord from 3-month-old *Opa3*^{+/-} and *Opa3*^{+/+} mice.

COX histochemistry

Mitochondrial activity was increased in the optic nerve of *Opa3*^{-/-} mice compared with *Opa3*^{+/+} mice (mean density 191.97 ± 5.74 versus 225.46 ± 2.4 , $P < 0.001$; Fig. 8C and D)

assessed by COX histochemistry (Old and Johnson, 1989). *Opa3*^{-/-} brain, which displayed evidence of degenerating axons by EM, showed no difference in COX activity in the corpus callosum compared to *Opa3*^{+/+} mice.

Discussion

In this study, we describe for the first time the generation and characterization of a novel ENU-induced mutant mouse with a clinical phenotype reminiscent of MGA Type III and carrying a mutation in the *opa3* gene. In the heterozygote state, the mutant mice (*Opa3*^{+/-}), are clinically and pathologically indistinguishable from

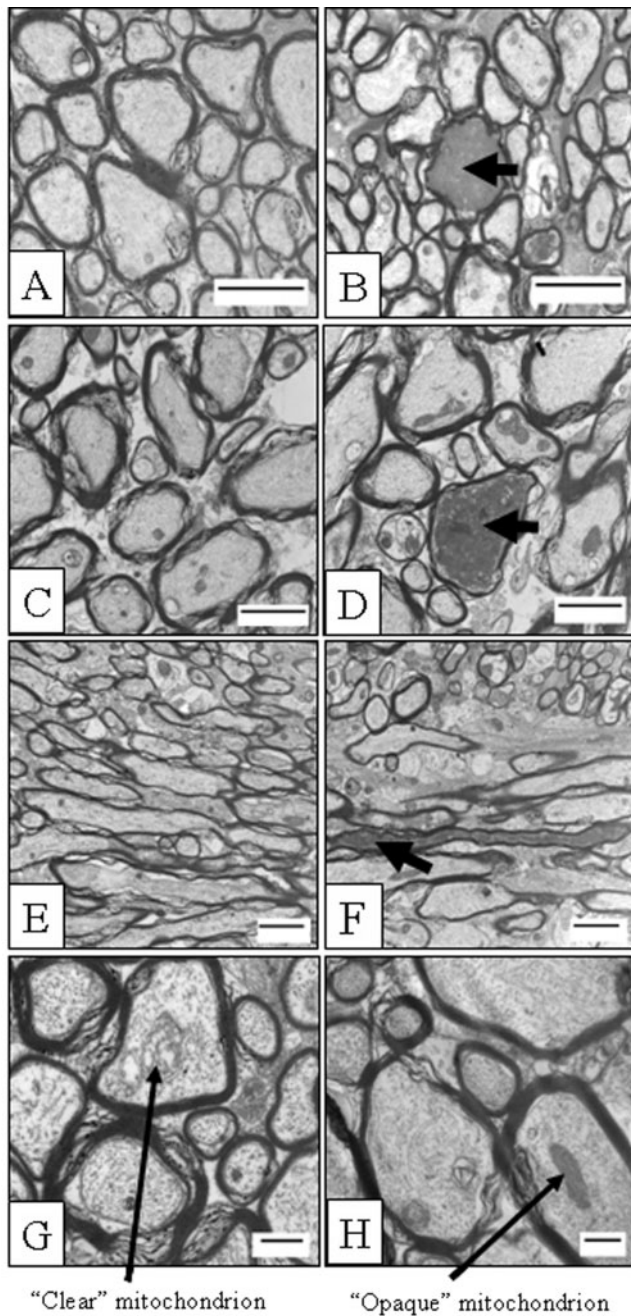


Fig. 7 Transmission electron micrographs of optic nerves (A) and (B), spinal cord (C) and (D) and brain (E) and (F) taken from 3- to 4-month-old *Opa3*^{+/+} (A), (C) and (E) and *Opa3*^{-/-} (B), (D) and (F) mice. In *Opa3*^{-/-} mice degenerating axons (denoted by arrows) were observed in the optic nerve, spinal cord and brain. Mitochondria with an opaque, densely stained matrix were identified more frequently in sections from *Opa3*^{-/-} mice than in *Opa3*^{+/+} controls. (G) and (H) show examples of mitochondria with a 'clear' (G) and 'opaque' matrix (H), respectively. (7A–F: bar = 2 microns. 7G&H: bar = 500 nm.)

littermate controls. However, in the homozygote state (*Opa3*^{-/-}) the mutant mice are severely compromised. These mice are runted, display a marked tremor and piloerection, and have less core body fat. They present with

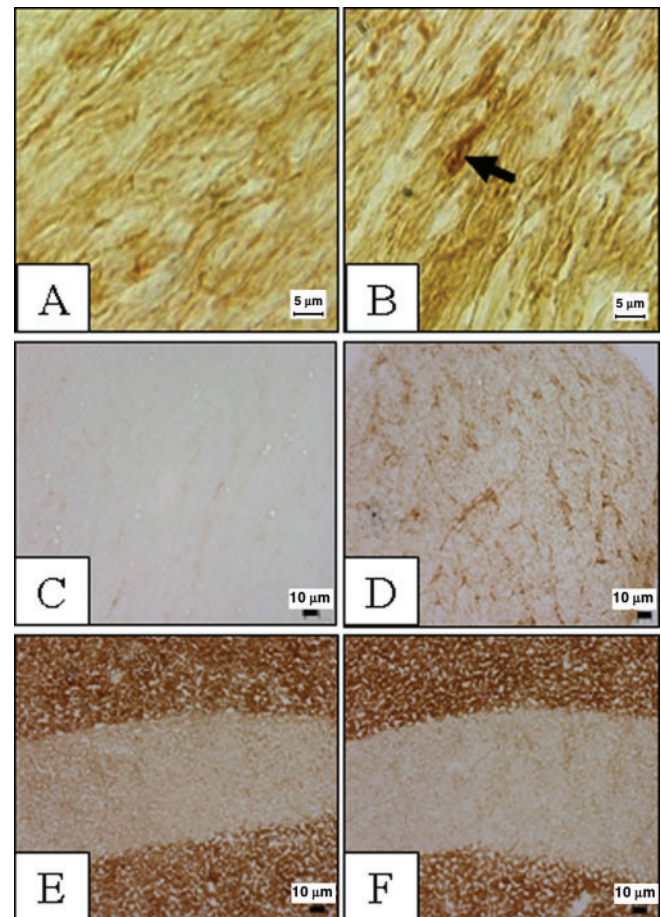


Fig. 8 (A) Neurofilament H (NF-H) immunostaining of *Opa3*^{+/+} optic nerve: degenerating axons identified in *Opa3*^{-/-} optic nerve sections (B) contained NF-H staining (denoted by arrow), consistent with 'dark' degeneration. Increased mitochondrial activity, demonstrated by COX histochemistry, was also identified in sections taken from *Opa3*^{-/-} (D) compared to *Opa3*^{+/+} (C) optic nerve. No difference in COX histochemistry in the brain of *Opa3*^{+/+} (E) and *Opa3*^{-/-} (F) animals was observed (the unstained area is the corpus callosum).

a splayed gait and limited movement. Their reduced visual acuity is consistent with the thinning of various retinal layers and a significant reduction in RGCs, extending to a distinct degeneration of axons within the optic nerve. The majority of these mutant mice fail to live beyond 4 months of age, possibly as a direct consequence of cardiomyopathy. The phenotype of the homozygous mice is variable and, in a few instances, these mice are identical in appearance to their littermates at weaning; however, their health status declines rapidly thereafter.

Mutations in the *OPA3* gene cause two distinct diseases in humans, which share some common characteristics. Similar to the clinical phenotype of ADOAC (5) and Type III MGA (Anikster *et al.*, 2001), our *Opa3*^{-/-} mice lose retinal ganglion cells leading to optic atrophy and reduced visual acuity. However, the detrimental mouse phenotype is only observed in the recessive state, and thus is not a

consequence of a dominantly inherited missense mutation, as is the case for ADOAC. Furthermore, there is no evidence of any type of cataract, a key characteristic of ADOAC (Reynier *et al.*, 2004) in the homozygote mice up to 4 months of age or in the heterozygote mutant mice up to 12 months of age; although we cannot exclude the possibility that cataract would develop with age thereafter. Moreover, our *Opa3*^{-/-} mutant mice do develop many of the other clinical features of MGA Type III (Anikster *et al.*, 2001; Kleta *et al.*, 2002). Through the SHIRPA neurological screen we observed symptoms that could be interpreted as spasticity (due to their abnormal gait and locomotion), extrapyramidal dysfunction (due to their reduced and inability to initiate movement) and ataxia (due to their splayed gait and unsteady motion of hind limbs). In addition, this phenotype is apparent in the recessive progeny, since their heterozygous parents are unaffected. These results indicate that the mode of inheritance is analogous to MGA Type III.

The missense mutation we have modelled is located in exon 2. The two mutations reported in ADOAC c.277G>A and c.313C>G are also located in exon 2 and may have a dominant negative effect causing a phenotype in the heterozygous state (Reynier *et al.*, 2004). The homozygous mutations that are causal in Type III MGA either abolish *OPA3* mRNA expression through a splice site mutation (Anikster *et al.*, 2001), or cause a homozygous 18-bp deletion in exon 2 of the *OPA3* gene, resulting in deletion of six amino acids between codons 108 and 113 (Kleta *et al.*, 2002), both of which result in loss of function. The effect of the p.L122P missense mutation on *OPA3* protein, introducing a proline residue, would be to alter the protein's tertiary structure causing disruption to its α -helix and β -sheet conformation (Silvestri *et al.*, 2005). This could have far reaching consequences for the function of the protein.

OPA3 mRNA is widely expressed throughout the body: most abundantly in the skeletal muscle, kidney and brain. The multi-systemic phenotype displayed by our *Opa3*^{-/-} mice is consistent with this expression. Results from this and other studies may implicate a function related to mitochondrial activity. Mitochondrial disorders affect high-energy consuming structures such as the basal ganglia, cerebellum, neurons and primary retinal ganglion cells, causing ataxia and optic atrophy (Kaplan, 2002; Chen and Chan, 2006), consistent with the phenotype of our *Opa3* mice. Many of their phenotypic characteristics and mode of inheritance are shared by other diseases caused by mutations that code for mitochondrial-related proteins; for example: ADOA (Alexander *et al.*, 2000; Delettre *et al.*, 2000), Charcot–Marie–Tooth disease type 2A (CMT2A; Zuchner *et al.*, 2006), type 4A (Pedrola *et al.*, 2005) Friedreich's ataxia (FRDA; Puccio and Koenig, 2000) and hereditary motor and sensory neuropathy type VI (HMSN VI; Zuchner *et al.*, 2004). Furthermore, it is known that *OPA3* contains a mitochondrial targeting sequence

(Anikster *et al.*, 2001) and localizes to the inner mitochondrial membrane (Da Cruz *et al.*, 2003). This allows us to speculate that the *OPA3* protein either belongs to the family of proteins involved in mitochondrial homeostasis, or it is involved in one of the many mitochondrial pathways. Future studies into the subcellular localization of the *OPA3* protein will provide us with a greater insight into the function of the protein.

The major characteristic of this mouse model is the loss of cells in all retinal layers, in particular the significant loss in the RGC layer, leading to optic atrophy and resulting in reduced visual acuity. From this, we are able to speculate that in the mouse, *OPA3* is expressed in the optic nerve, and the various layers of the retina, in particular the RGC layer, and that it is important in either retinal development or maintenance. Further work will be needed to distinguish between these two mechanisms and to characterize the developmental expression profile of *Opa3* in the retina.

Mitochondria are concentrated in the non-myelinated parts of optic nerve axon, optic nerve head and just past the lamina cribrosa, as well as at the nodes of Ranvier. Axonal transport is an ATP-dependent process, mitochondria being the major source of this ATP (Carelli *et al.*, 2002), thereby providing an explanation for increased mitochondrial activity in the unmyelinated axons (Barron *et al.*, 2004). In our *Opa3*^{-/-} mice we observed increased mitochondrial activity in the post-laminar myelinated region of the optic nerve, demonstrated by increased COX histochemistry. This was not because of demyelination or increased numbers of mitochondria, as neither was observed, but might be a direct consequence of inefficient mitochondria increasing their activity to meet energy demand following the degeneration of optic nerve axons. Adaptive changes involving the mitochondria take place in the optic nerve axon; in the *Shiverer* mouse, dysmyelination results in a higher number of mitochondria within the axon in response to the lack of myelin (Andrews *et al.*, 2006). This increased energy requirement also promotes the production of reactive oxygen species in mitochondria, which damage the axons further (Andrews *et al.*, 2006). There is extensive evidence of degenerating axons in our *Opa3*^{-/-} mice, consistent with the consequences of increased mitochondrial activity. However, consistent with the published literature (Gallyas *et al.*, 2006) the myelin sheaths surrounding these degenerating axons remained unchanged. This type of degeneration has been classified as 'dark' degeneration; the axons contain a dense axoplasm (Marques *et al.*, 2003). In our *Opa3*^{-/-} model, the dark degenerating axons coincided with increased NF staining, in accord with NF proteins participating in the process of axonal dark degeneration (Marques *et al.*, 2003).

The cause of early death in our *Opa3*^{-/-} mice is not immediately apparent; they die suddenly in the absence of preceding illness, undue stress or fasting. If the *OPA3* protein is linked with mitochondrial function or processes, mitochondrial dysfunction may be the cause of their

lethality. Cardiomyopathy could be the primary cause of their death, or it could be a secondary consequence of either mitochondrial dysfunction or multiple organ failure. At the time of illness and death, our *Opa3*^{-/-} mice are severely dehydrated (making urine collection impossible) and have a near complete absence of internal body fat, despite the kidneys appearing normal by histological analysis and being witnessed drinking and eating normally.

In summary, we describe a novel mutant mouse B6; C3-*Opa3*^{L122P}, which displays bilateral optic atrophy, reduced visual acuity, extrapyramidal dysfunction, spasticity, ataxia and a shortened life span. This novel mouse will be a valuable tool, providing a means to investigate directly the functional role of *Opa3* *in vivo* and the pathophysiology of both Type III MGA.

Acknowledgements

The authors would like to thank Ingenium Pharmaceuticals for ENU mutagenesis and IVF, Ruby Grewal for assistance with genotyping, and Dr Pawel Tokarczuk and Dr Stuart Faulkner for MRI in the Cardiff University MRI facility. This work was funded by a grant from the Medical Research Council.

References

- Alexander C, Votruba M, Pesch UE, Thiselton DL, Mayer S, Moore A, et al. OPA1, encoding a dynamin-related GTPase, is mutated in autosomal dominant optic atrophy linked to chromosome 3q28. *Nat Genet* 2000; 26: 211–5.
- Andrews H, White K, Thomson C, Edgar J, Bates D, Griffiths I, et al. Increased axonal mitochondrial activity as an adaptation to myelin deficiency in the Shiverer mouse. *J Neurosci Res* 2006; 83: 1533–9.
- Anikster Y, Kleta R, Shaag A, Gahl WA, Elpeleg O. Type III 3-methylglutaconic aciduria (optic atrophy plus syndrome, or Costeff optic atrophy syndrome): identification of the OPA3 gene and its founder mutation in Iraqi Jews. *Am J Hum Genet* 2001; 69: 1218–24.
- Barron MJ, Griffiths P, Turnbull DM, Bates D, Nichols P. The distributions of mitochondria and sodium channels reflect the specific energy requirements and conduction properties of the human optic nerve head. *Br J Ophthalmol* 2004; 88: 286–90.
- Carelli V, Ross-Cisneros FN, Sadun AA. Optic nerve degeneration and mitochondrial dysfunction: genetic and acquired optic neuropathies. *Neurochem Int* 2002; 40: 573–84.
- Chen H, Chan DC. Critical dependence of neurons on mitochondrial dynamics. *Curr Opin Cell Biol* 2006; 18: 453–9.
- Cipolat S, Martins de Brito O, Dal Zilio B, Scorrano L. OPA1 requires mitofusins 1 to promote mitochondrial fusion. *Proc Natl Acad Sci USA* 2004; 101: 15927–32.
- Da Cruz S, Xenarios I, Langridge J, Vilbois F, Parone PA, Martinou JC. Proteomic analysis of the mouse liver mitochondrial inner membrane. *J Biol Chem* 2003; 278: 41566–71.
- Davies VJ, Hollins AJ, Piechota MJ, Yip W, Davies JR, White KE, et al. Opa1 deficiency in a mouse model of autosomal dominant optic atrophy impairs mitochondrial morphology, optic nerve structure and visual function. *Hum Mol Genet* 2007; 16: 1307–18.
- Delettre C, Lenaers G, Griffoin JM, Gigarel N, Lorenzo C, Belenguer P, et al. Nuclear gene OPA1, encoding a mitochondrial dynamin-related protein, is mutated in dominant optic atrophy. *Nat Genet* 2000; 26: 207–10.
- Gallyas F, Pal J, Farkas O, Doczi T. The fate of axons subjected to traumatic ultrastructural (neurofilament) compaction: an electron-microscopic study. *Acta Neuropathol (Berl)* 2006; 111: 229–37.
- Garcin R, Raverdy P, Delthil S, Man HX, Chimenes H. On a heredo-familial disease combining cataract, optic atrophy, extrapyramidal symptoms and certain defects of Friedreich's disease. (Its nosological position in relation to the Behr's syndrome, the Marinesco-Sjogren syndrome and Friedreich's disease with ocular symptoms). *Rev Neurol* 1961; 104: 373–9.
- Gimenez E, Montoliu L. A simple polymerase chain reaction assay for genotyping the retinal degeneration mutation (Pdeb(rd1)) in FVB/N-derived transgenic mice. *Lab Anim* 2001; 35: 153–6.
- Griparic L, van der Wel NN, Orozco IJ, Peters PJ, van der Blik AM. Loss of the intermembrane space protein Mgm1/OPA1 induces swelling and localized constrictions along the lengths of mitochondria. *J Biol Chem* 2004; 279: 18792–8.
- Hart AW, McKie L, Morgan JE, Gautier P, West K, Jackson IJ, et al. Genotype-phenotype correlation of mouse *pde6b* mutations. *Invest Ophthalmol Vis Sci* 2005; 46: 3443–50.
- Kaplan J. Spinocerebellar ataxias due to mitochondrial defects. *Neurochem Int* 2002; 40: 553–7.
- Kjer P. Infantile optic atrophy with dominant mode of inheritance: a clinical and genetic study of 19 Danish families. *Acta Ophthalmol Suppl* 1959; 164: 1–147.
- Kleta R, Skovby F, Christensen E, Rosenberg T, Gahl WA, Anikster Y. 3-methylglutaconic aciduria type III in a non-Iraqi-Jewish kindred: clinical and molecular findings. *Mol Genet Metab* 2002; 76: 201–6.
- Marques SA, Taffarel M, Blanco Martinez AM. Participation of neurofilament proteins in axonal dark degeneration of rat's optic nerves. *Brain Res* 2003; 969: 1–13.
- Nystuen A, Costeff H, Elpeleg ON, Apter N, Bonne-Tamir B, Mohrenweiser H, et al. Iraqi-Jewish kindreds with optic atrophy plus (3-methylglutaconic aciduria type 3) demonstrate linkage disequilibrium with the CTG repeat in the 3' untranslated region of the myotonic dystrophy protein kinase gene. *Hum Mol Genet* 1997; 6: 563–9.
- Old SL, Johnson MA. Methods of microphotometric assay of succinate dehydrogenase and cytochrome c oxidase activities for use on human skeletal muscle. *Histochem J* 1989; 21: 545–55.
- Olichon A, Baricault L, Gas N, Guillou E, Valette A, Belenguer P, et al. Loss of OPA1 perturbs the mitochondrial inner membrane structure and integrity, leading to cytochrome c release and apoptosis. *J Biol Chem* 2003; 278: 7743–6.
- Pedrola L, Espert A, Wu X, Claramunt R, Shy ME, Palau F. GDAP1, the protein causing Charcot-Marie-Tooth disease type 4A, is expressed in neurons and is associated with mitochondria. *Hum Mol Genet* 2005; 14: 1087–94.
- Puccio H, Koenig M. Recent advances in the molecular pathogenesis of Friedreich ataxia. *Hum Mol Genet* 2000; 9: 887–92.
- Qiao X, Pennesi M, Seong E, Gao H, Burmeister M, Wu SM. Photoreceptor degeneration and rd1 mutation in the grizzled/mocha mouse strain. *Vision Res* 2003; 43: 859–65.
- Reynier P, Amati-Bonneau P, Verny C, Olichon A, Simard G, Guichet A, et al. OPA3 gene mutations responsible for autosomal dominant optic atrophy and cataract. *J Med Genet* 2004; 41: e110.
- Rogers DC, Fisher EM, Brown SD, Peters J, Hunter AJ, Martin JE. Behavioral and functional analysis of mouse phenotype: SHIRPA, a proposed protocol for comprehensive phenotype assessment. *Mamm Genome* 1997; 8: 711–3.
- Silvestri L, Caputo V, Bellacchio E, Atorino L, Dallapiccola B, Valente EM, et al. Mitochondrial import and enzymatic activity of PINK1 mutants associated to recessive parkinsonism. *Hum Mol Genet* 2005; 14: 3477–92.
- Thaug C, Arnold K, Jackson IJ, Coffey PJ. Presence of visual head tracking differentiates normal sighted from retinal degenerate mice. *Neurosci Lett* 2002; 325: 21–4.

Votruba M, Moore AT, Bhattacharya SS. Demonstration of a founder effect and fine mapping of dominant optic atrophy locus on 3q28-qter by linkage disequilibrium method: a study of 38 British Isles pedigrees. *Hum Genet* 1998a; 102: 79–86.

Votruba M, Payne A, Moore AT, Bhattacharya SS. Dominant optic atrophy: exclusion and fine genetic mapping of the candidate gene, HRY. *Mamm Genome* 1998b; 9: 784–7.

Zuchner S, De Jonghe P, Jordanova A, Claeys KG, Guergueltcheva V, Cherninkova S, et al. Axonal neuropathy with optic atrophy is caused by mutations in mitofusin 2. *Ann Neurol* 2006; 59: 276–81.

Zuchner S, Mersyanova IV, Muglia M, Bissar-Tadmouri N, Rochelle J, Dadali EL, et al. Mutations in the mitochondrial GTPase mitofusin 2 cause Charcot-Marie-Tooth neuropathy type 2A. *Nat Genet* 2004; 36: 449–51.